HHS Public Access

Author manuscript

Radio Sci. Author manuscript; available in PMC 2017 August 23.

Published in final edited form as:

Radio Sci. 2017 July 12; 52(6): 731–742. doi:10.1002/2016RS006242.

Mathematical modeling and measurement of electric fields of electrode-based through-the-earth (TTE) communication

Lincan Yan[1], **Chenming Zhou**[1], **Miguel Reyes**[1], **Bruce Whisner**[1], and **Nicholas Damiano**[1]

[1]Pittsburgh Mining Research Division, National Institute for Occupational Safety and Health, Pittsburgh, Pennsylvania, USA

Abstract

There are two types of through-the-earth (TTE) wireless communication in the mining industry: magnetic loop TTE and electrode-based (or linear) TTE. While the magnetic loop systems send signal through magnetic fields, the transmitter of an electrode-based TTE system sends signal directly through the mine overburden by driving an extremely low frequency (ELF) or ultralow frequency (ULF) AC current into the earth. The receiver at the other end (underground or surface) detects the resultant current and receives it as a voltage. A wireless communication link between surface and underground is then established. For electrode-based TTE communications, the signal is transmitted through the established electric field and is received as a voltage detected at the receiver. It is important to understand the electric field distribution within the mine overburden for the purpose of designing and improving the performance of the electrode-based TTE systems. In this paper, a complete explicit solution for all three electric field components for the electrode-based TTE communication was developed. An experiment was conducted using a prototype electrode-based TTE system developed by National Institute for Occupational Safety and Health. The mathematical model was then compared and validated with test data. A reasonable agreement was found between them.

1. Introduction

Through-the-earth (TTE) wireless communication provides an alternate way for trapped miners and rescue personnel to communicate in case of emergency in underground mines. There are two types of TTE wireless communication systems currently available for the mining industry: the electrode-based TTE system and the magnetic loop TTE system. Compared to the magnetic loop system, the electrode-based system has fewer components and can achieve stable communication and transmit across a long range. While the magnetic loop system sends signal through magnetic fields, the electrode-based system utilizes the electric field generated by the transmitter (TX) wire antenna within the earth overburden. This kind of TTE system must be capable of operating under a variety of geological conditions that may impact performance.

One of the challenges confronting system designers is to design a system that will operate in all underground coal mines, including mines that have large overburden depth (>914 mor

Correspondence to: L. Yan, lyan1@cdc.gov.

3000 ft). The understanding of the electric field distribution within the overburden is therefore important for the design and application of electrode-based TTE systems. Over the past few decades, researchers have investigated the electromagnetic fields within the earth due to an ELF or ULF source on the surface [*Wait*, 1961; *Wait and Spies*, 1971; *Persinger*, 1974; *Geyer et al.*, 1974; *Gibson*, 2003]. The static electric field was obtained for a line source carrying DC current [*Geyer et al.*, 1974; *Yan and Sunderman*, 2015]. Wait and Spies developed a two-dimensional model to evaluate the electromagnetic fields within the earth due to an infinite line source carrying an ELF/ULF AC current on the surface [*Wait and Spies*, 1971]. *Bataller et al.* [2010] proposed an optimal circuit model for earth impedance between electrodes as a function of frequency for electrode-based TTE communication applications.

In this paper, a three-dimensional model of the subsurface electric fields was developed based on *Hill and Wait*'s [1973] work. The model was then used to characterize the factors that will affect the electric field distribution—hence the voltage detected at the RX. These factors include TX and RX offset and relative orientation, the length of the TX and RX, mine overburden depth, apparent earth conductivity of the mine, and operating frequency. Of those factors, some might be chosen appropriately to establish or improve the communication link. The analytical model also was compared with test data collected at a coal mine using a prototype electrode-based TTE system developed by researchers at the National Institute for Occupational Safety and Health (NIOSH) [*Yan et al.*, 2016].

2. Explicit Form of Electric Fields

The subsurface electric fields of an infinite cable carrying a current have been given by *Wait and Spies* [1971]. In a TTE communication link, however, the transmit cable or antenna has a finite length. A finite length cable that carries a current with a magnitude of I and angular frequency of ω is shown in Figure 1. The cable is situated at ground and has a length of 2 l. The earth medium is homogenous. All displacement currents can be ignored since operating frequency is in the ultralow- or extralow-frequency range. While the behavior of electromagnetic fields at high frequencies is due partly to propagation effects and is characteristic of wave theory, the fields at low frequencies such as TTE are more easily addressed using potential theory. The magnetic potential, Π, due to a current source with infinitesimal length dx' is given by [*Wait*, 1961]

$$\{d\Pi_x, d\Pi_y, d\Pi_z\} = \frac{I dx'}{2\pi\sigma\gamma^2}\left\{\frac{\partial^2 P}{\partial z^2} - \frac{\partial^3 N}{\partial z^3} + \gamma^2\frac{\partial N}{\partial z}, 0, \frac{\partial^3 N}{\partial x \partial z^2} - \frac{\partial^2 P}{\partial x \partial z}\right\} \quad (1)$$

where $N = I_0[(R+z)\gamma/2]K_0[(R-z)\gamma/2]$, $P = e^{-\gamma R}/R$, $\gamma^2 = j\omega\mu_0\sigma$, $\rho = \sqrt{y^2+(x-x')^2}$, $R = \sqrt{\rho^2+z^2}$, μ_0 is the permeability of free space, σ is the earth conductivity, j is the square root of −1, I_0 is the modified Bessel function of the first kind of order zero with the argument of $(R+z)\gamma/2$, and K_0 is the modified Bessel function of the second kind of order zero with the argument of $(R-z)\gamma/2$.

The electric field relates to magnetic potential through

$$\boldsymbol{E}=-\gamma^2\boldsymbol{\Pi}+\nabla(\nabla\cdot\boldsymbol{\Pi}) \quad (2)$$

In a Cartesian coordinates system, all three components of $\boldsymbol{E}$ are expressed as

$$\{dE_x, dE_y, dE_z\}=\frac{-Idx'}{2\pi\sigma}\left\{\frac{\partial^2 P}{\partial z^2}+\frac{\partial^3 N}{\partial y^2\partial z}, \frac{-\partial^3 N}{\partial x\partial y\partial z}, \frac{\partial^2 P}{\partial x\partial z}\right\} \quad (3)$$

The partial derivatives of P and N in (3) with respect to x, y, and z are listed in the Appendix. For ELF (<30 Hz) or DC current source, $\gamma^2 = j\omega\mu_0\sigma\rightarrow 0$. The magnetic potential in (1) can be rewritten as

$$d\Pi_x=\frac{Idx'}{4\pi\sigma}\frac{1}{R} \quad (4)$$

$$d\Pi_y=0 \quad (5)$$

$$d\Pi_z=\frac{-Idx'}{4\pi\sigma}\frac{(x-x')}{\rho^2}(1+z/R) \quad (6)$$

The electric fields due to an ELF or DC current source with infinitesimal length dx' is then given by taking the operation in (2) and setting $\gamma = 0$, i.e.,

$$dE_x=\frac{I\left(2x^2-4xx'+2x'^2-y^2-z^2\right)}{2\pi\sigma(x^2-2xx'+x'^2+y^2+z^2)^{5/2}}dx' \quad (7)$$

$$dE_y=\frac{3I(x-x')y}{2\pi\sigma(x^2-2xx'+x'^2+y^2+z^2)^{5/2}}dx' \quad (8)$$

$$dE_z = \frac{3I(x-x')z}{2\pi\sigma(x^2-2xx'+x'^2+y^2+z^2)^{5/2}}dx' \quad (9)$$

Integrating (7)–(9) over the entire length of the TX from $-l$ to l, we have all three electric field components at point $P(x, y, z)$.

$$E_x = \frac{I}{2\pi\sigma}\left(\frac{-I+x}{(I^2-2Ix+x^2+y^2+z^2)^{3/2}} - \frac{I+x}{(I^2+2Ix+x^2+y^2+z^2)^{3/2}}\right) \quad (10)$$

$$E_y = \frac{I\,y}{2\pi\sigma}\left(\frac{1}{(I^2-2Ix+x^2+y^2+z^2)^{3/2}} - \frac{1}{(I^2+2Ix+x^2+y^2+z^2)^{3/2}}\right) \quad (11)$$

$$E_z = \frac{I\,z}{2\pi\sigma}\left(\frac{1}{(I^2-2Ix+x^2+y^2+z^2)^{3/2}} - \frac{1}{(I^2+2Ix+x^2+y^2+z^2)^{3/2}}\right) \quad (12)$$

Note that (10) and (11) are exactly the same as what were given in *Geyer et al.* [1974] and *Yan and Sunderman* [2015]. For a horizontal oriented RX, the received voltage at RX is obtained by integrating (10) and (11) over the entire length of RX.

$$V_{Rx}(x, y, \theta) = \int_{-I}^{I}(E_x\cos\theta + E_y\sin\theta)dI' \quad (13)$$

The induced voltage, hence the transmitted signal strength, received at the RX is affected by several factors including earth conductivity, overburden depth, operating frequency, TX/RX antenna length, TX/RX offset, TX/RX angle, and TX current. The effect of those parameters on E-field strength will be discussed as below.

2.1. TX/RX Offset

In practice, the center of the TX and RX of a TTE system may not be perfectly aligned—i.e., there might be an offset either in the y direction (parallel) or the x direction (coaxial), as shown in Figure 2. The analytical model presented in this paper provides us with a tool to investigate how a TTE system is affected by the TX/RX offset. Based on (3), the received voltage at the RX is calculated and plotted against normalized TX/RX coaxial distance (x_0/h) for various offsets y_0 in Figure 3. Figure 3 shows that the received voltage decreases when the RX is moving away from the TX. A null appears in this TX/RX arrangement. This suggests possible poor signal reception if the RX is sited at the null locations.

It can be observed from Figure 3 that the received voltage at RX is not extremely sensitive to offset value when this value is relative small. For example, there is only approximately 0.2 dBV difference between $y_0 = 2$ L and $y_0 = 0$.

2.2. TX/RX Orientation Angle

Similar to the TX/RX offset, another factor that can affect TTE system performance is the TX/RX orientation angle, as TX and TX may not be deployed parallel to each other due to practical constraints. As shown in Figure 4, the RX centered at $P(x_0, y_0, z = -h)$ has an angle θ related to the TX. Both x and y components of the E field should be considered at the receiver, and the received voltage can be calculated based on (3) and (13).

The calculated voltage at the RX for different TX/RX intersection angles (θ) at various RX locations is given in Figure 5. At $x_0 = y_0 = 0$, the RX is sited directly underneath the TX. The RX voltage decreases with angle θ. Minimal voltage will be produced at the RX when it is perpendicular to the TX ($\theta = 90°$) at this location. When the RX and TX are not coplanar, i.e., they are horizontally offset in x-y plane, however, rotating the RX so that it forms an angle with the TX may achieve a maximum voltage at the RX. This is because the x component of the E field is dominant when TX and RX are vertically aligned, then the y component of the E field becomes dominant when TX and RX are horizontally separated by a considerably large distance (>6 L). Figure 6 shows how the ratio of x-component E field (E_x) to y-component E field (E_y) varies with RX locations P. The x-component E field is the dominant field when RX and TX are vertically aligned (i.e., the RX is directly underneath the TX). That ratio decreases when the RX is moving away horizontally from the TX. When the horizontal separation distance between RX and TX is large (>0.6 h), the y component becomes the dominant field.

2.3. Overburden Depth

Figure 7 shows how the earth overburden depth affects the electrical field at a given earth conductivity at different frequencies. Again, the electrical field is normalized to the transmitting current. It is apparent from Figure 7 that electrical field at a fixed frequency decreases with overburden depth monotonically. In other words, it would be more challenging to establish a reliable TTE communication link in deeper mines. Since the decreasing rate of the E field with respect to depth increases with frequency, a TTE system operating at lower frequencies is likely to have a better chance to work in deep mines.

2.4. Earth Conductivity

Figure 8 shows how the earth conductivity affects the electrical field at a given depth at different frequencies. The y axis of Figure 8 is the horizontal E field (E_x) normalized to the transmitting current. The other parameters used in the simulation include: $x = 0$, $y = 0$, $z = -h = -100$ m, and $L = 76$ m. As shown in Figure 8, for a given frequency, the horizontal E field decreases with conductivity. The decreasing rate of the E field with respect to the earth conductivity, however, generally increases with frequency. This indicates that for mines with high apparent conductivity, low operating frequencies should always be chosen in order to decrease earth attenuation and to achieve the received RX voltage required for a reliable wireless communication link. It should also be noted that for mines with high earth

conductivity value, the lowest frequency (20 Hz) does not achieve the highest E field (e.g., σ = 0.4 S/m in Figure 8). It indicates that there is an optimum frequency that can yield the maxim E field when other controlling factors are fixed.

2.5. TX and RX Antenna Length

When the TX is transmitting, the received voltage at RX is obtained via integrating the E field along the entire length of the RX. So the RX antenna length will affect the magnitude of the voltage received at RX. Figure 9a shows that the RX voltage changes with RX length (2Lrx) for different TX antenna length (2Ltx). For a given TX antenna length, increasing RX length will increase RX voltage. However, the increasing rate decreases and finally stops when the RX length gets sufficiently larger (Lrx/h > 0.8 h). For an electrode-based TTE system, the transceiver usually uses one wire antenna for both transmitting and receiving. Similarly, as shown in Figure 9b, increasing the TX length can also increase the received voltage at RX. Increasing the TX antenna length, however, is restricted by the difficulty in maintaining the required TX current.

2.6. Operating Frequency

For TTE communication, the operating frequency should be chosen appropriately so a reliable communication link can be established. Figure 10 shows the electric field changing with operating frequency for different apparent conductivities. Similar in air space, the resultant electric field increases with operating frequency at low apparent conductivities (σ < 0.01S/m). For mine sites having higher apparent conductivities (σ > 0.01S/m), however, increasing the operating frequency in the ELF or ULF range will not necessarily increase the electric field at RX, given other parameters remaining the same. Instead, an “optimal” operating frequency may exist for high earth conductivity between 100 and 500 Hz. For a conductive medium, as in a magnetic loop TTE system, high frequency will result in high attenuation since the skin depth gets smaller. However, for a free space or very low conductive medium, the higher frequency will achieve higher SNR, provided other conditions remain the same. That “optimal” peak might be an outcome of this trade-off.

2.7. Transmitter Current

As (3) implies, the E field at a receiver is proportional to the transmitter current. This means that when the transmitter current is maximized, the signal reception at the receiver is optimal. It should be noted, though not shown in (3), that the contact impedance of grounding rods (i.e., the electrodes) at the transmitter side will affect transmitter current and thus influence the signal reception at the receiver as well. More details on the effect of contact impedance of grounding rods on electrode-based TTE communication can be found in *Damiano et al.* [2016].

3. Experiment

In order to evaluate the earth attenuation, communication reliability, and transmission range of electrode-based TTE systems, researchers at NIOSH conducted experiments at a coal mine site using a prototype electrode-based TTE system developed by NIOSH. The test data were then used to validate the model previously developed.

3.1. Test Setup

As shown in Figure 11, the TTE system includes an amplifier; an analog to digital converter; a pair of electrodes, each consisting of eight grounding rods; and a laptop with the LabVIEW program installed. As a transceiver (TCVR), the system acts as both transmitter and receiver. When transmitting, the current and voltage across the electrodes were monitored using a passive current sensor (model no. BCP-510 by AH Systems) and a high-resolution resistor, respectively. When receiving, the voltage induced across the electrodes was displayed and recorded for post processing. Two systems were used during the test—one for uplink (underground to surface) transmission and one for downlink (surface to underground) transmission.

As depicted in Figure 12, four locations were selected to conduct vertical and diagonal transmission tests—two at Location 1 (UG1 underground and AG1 at surface) and two at Location 2 (UG2 underground and AG2 at surface). UG1 and AG1 and UG2 and AG2 are vertically aligned. The overburden depth is 149 m (490 ft) at Location 1 and 293 m (961 ft) at Location 2. The horizontal distance between Location 1 and Location 2 is about 2100 m (~7000 ft).

As shown in Figure 13, two types of electrode arrangements were used for underground and surface locations. Each electrode consists of eight copper grounding rods which are 1.59 cm (5/8 inch) in diameter and 1.22 m (4 ft) long. Those grounding rods were evenly separated with a spacing of 2.44 m (8 ft) and inserted into the ground 1.07 m–1.22 m (3.5 ft–4 ft) deep. A copper (II) sulfate ($CuSO_4$) solution was used to improve the conductivity of grounding rods to the earth (Figure 13b). At each test location, the electrode pair was separated by a distance of ~76 m (250 ft). More details on the effect of grounding rod deployment (rod connection configuration, spacing, inserted depth, number of rods, etc.) on electrode-based TTE communication can be found in *Damiano et al.* [2016].

3.2. Test Results

Of the parameters that will affect the electrode-based TTE communication as discussed previously, some were changed during the test to experimentally investigate their effects on signal strength—i.e., the voltage received by the RX. Several operating frequencies were selected to look at the optimal frequency that may exist. To avoid 60 Hz harmonics which appeared in the background noise, seven operating frequencies were chosen: 20, 100, 330, 450, 610, 990, and 3030 Hz. The TX voltage delivered on the electrodes when transmitting —hence the transmitting current—was adjusted in magnitude for each operating frequency. At each pair of locations, transmission was made for both downlink and uplink to investigate the signal reciprocity for electrode-based TTE communication. The earth resistance between two electrodes at all four test locations was measured to estimate the required output voltage for the TTE transmission at those locations. As reflected in (3), the signal strength at the RX depends on the transmitting current *I*. While increasing the TX voltage is restricted by safety concerns, one feasible way to increase transmitting current is to reduce the earth resistance between the pair of electrodes. By adding the copper sulfate solution into ground as shown in Figure 13, the earth resistance can be fairly reduced. The measured earth resistances with copper sulfate solution added at all test locations are listed as in Table 1.

Two electrode-based TTE systems were used to conduct vertical uplink and vertical downlink transmission tests at Location 1 and Location 2—one for underground and one for surface. The received voltage at the RX for different operating frequencies at Location 1 is shown in Figure 14, for both uplink and downlink. As Figure 14 shows, when transmitting current I changes, the RX voltage will change accordingly (curves labeled as V1 through V4). For downlink transmission, an optimal frequency might exist in the range of 100 Hz–500 Hz, as shown in Figure 14a. For uplink transmission (Figure 14b), the RX could not detect any signal at frequencies of 990 Hz and 3030 Hz.

Both TTE systems were then moved to Location 2 which has a larger overburden depth. The received voltage at the RX for different operating frequencies at Location 2 is shown in Figure 15. As expected, the signal strength is much weaker due to the large overburden depth at this location, given the same transmitting current as used at Location 1. For the same reason, the higher frequencies (>610 Hz) could not be detected by the RX. Similarly, as at Location 1, an optimal frequency might exist in the range of 20–300 Hz at Location 2.

The first diagonal transmission was made between AG1 and UG2 with a distance of 2140 m approximately. The received voltage at the RX for different operating frequencies is shown in Figure 16. Similarly, the higher frequencies (>450 Hz) could not be detected by the RX due to the large overburden depth. Also, an optimal frequency might exist in the range of 20–300 Hz for the transmission link between AG1 and UG2.

The second diagonal transmission was made between AG2 and UG1 with a distance of approximately 2153 m. Of all seven operating frequencies, only two (20 Hz and 100 Hz) were detected by the RX for uplink transmission. No frequency was detected for the downlink transmission. The reason could be the relatively high earth resistance at AG2 which restricts the transmitting current.

The signal propagation is not necessarily reciprocal during magnetic loop TTE communications, especially when the apparent earth conductivity is high [*Persinger*, 1974; *Yan et al.*, 2013]. For electrode-based TTE communication, however, *Hill and Wait* [1973] and *Hill* [1973] obtained the same forms of the underground electric field and surface electric field due to a surface cable and a buried cable, respectively. The measured RX voltages normalized by the transmitting currents (V_{RX}/I_{TX}) are listed as in Table 2 for all available test conditions. The difference between uplink and downlink transmission is less than 1% for all cases. The test data confirm that the transmission is reciprocal for electrode-based TTE communication at that mine site.

4. Model Validation

The electric field strength, or the voltage received by the RX, will determine the performance or success of the communication link produced by an electrode-based TTE system. Before an electrode-based TTE system is installed at a mine, it is important to estimate the electric field distribution within the overburden to establish a TTE link by appropriately choosing parameters such as operating frequency, antenna length, and installation location. The model prediction compared with test data is shown in Figure 17 for

vertical transmission at Location 1 and Location 2. The RX voltage (V_{RX}) was normalized by the TX current (I_{TX}) to eliminate its effect for both model calculation and test data. The apparent earth conductivity (σ) was chosen to 0.2 S/m based on estimation of the electrical property of the mine stratigraphy. For all other parameters such as overburden depth and antenna length, the model calculation used the same value as what appeared in the test. At both locations, the model results agree with test data more closely at high frequencies than at lower frequencies. One explanation to the discrepancy between the model and test data at lower frequencies (<100 Hz) is the signal distortion by the receiver digitizer at lower frequencies. It is observed that in Figure 17, an optimal operating frequency exists in the range of 20–500 Hz at Location 1 and in the range of 20–300 Hz at Location 2 for both model prediction and test data. The figure also shows that the signal strength decreases dramatically with operating frequency at Location 2. In other words, it suggests that lower operating frequency should always be chosen at locations that have larger overburden depth.

5. Discussion and Conclusion

A three-dimensional model of the subsurface electric fields for electrode-based TTE communication was developed and examined for various factors that will affect received voltage at the RX. The analysis shows that increasing the electric field at the RX will increase with TX/RX antenna length before reaching its limit. The relative orientation of the TX and the RX (horizontal offset and intersection angle) can also change the electric field distribution pattern, and therefore the signal reception at RX. The maximum E field seen by the RX is obtained when the RX is parallel to and right underneath the TX. When the RX is horizontally offset away from the TX, however, rotating the RX so that TX and RX are perpendicular to each other may enhance the signal reception. A null also exists when the RX and TX are horizontally separated by a considerably large distance. An optimal operating frequency may exist if the mine's apparent earth conductivity is not considerably low.

Field test was conducted for various configurations at a coal mine site using a NIOSH-developed electrode-based TTE system. Signal was successfully transmitted across a considerably large distance of >2134 m (7000 ft). As expected in the model analysis, optimal operating frequency was observed during the test. The test also confirmed that the transmission is reciprocal for electrode-based TTE communication. The model was then compared with and validated by test data.

Finally, by understanding the controlling factors on the effect of the E fields, engineers can use the validated model to optimize system design through choices for the operating frequency, installation location, transmitting current, TX/RX orientation angle, and TX/RX offset to successfully establish and improve the performance of electrode-based TTE system at a mine based on its geologic characteristics.

Acknowledgments

Mention of a company name or product does not constitute an endorsement by the National Institute for Occupational Safety and Health. The findings and conclusions in this report are those of the authors and do not necessarily represent the views of the National Institute for Occupational Safety and Health. This article is not

References

Bataller V, MuñOz A, Gaudó PM, Mediano A, Cuchí JA, Villarroel JL. Earth impedance model for through-the-earth communication applications with electrodes. Radio Sci. 2010; 45:RS6015.doi: 10.1029/2010RS004406

Damiano, N., Yan, L., Whisner, B., Zhou, C. Simulation and measurement of through-the-earth (TTE), extremely low-frequency signals using copper-clad, steel ground rods. IEEE IAS Annual Meeting; Portland, Ore. 2016.

Geyer, R., Keller, G., Ohya, T. Research on the Transmission of Electromagnetic Signals Between Mine Workings and the Surface. Colo. School of Mines, Golden; 1974. p. 62-88.

Gibson, ADW. Channel Characterisation and System Design for Sub-surface Communications. Univ. of Leeds; Leeds, U. K: 2003. p. 24-58.

Hill D, Wait J. Subsurface electromagnetic fields of a grounded cable of finite length. Can J Phys. 1973; 51(14):1534–1540.

Hill DA. Electromagnetic surface fields of an inclined buried cable of finite length. J Appl Phys. 1973; 44(12):5275–5279.

Persinger, MA. ELF and VLF Electromagnetic Field Effects. Plenum Press; New York: 1974. p. 275-300.

Wait J. The electromagnetic fields of a horizontal dipole in the presence of a conducting half-space. Can J Phys. 1961; 39(7):1017–1028.

Wait J, Spies K. Subsurface electromagnetic fields of a line source on a conducting half-space. Radio Sci. 1971; 6(8–9):781–786.

Yan, L., Sunderman, C. Electric field of grounded horizontal line transmitter for through the earth communication. The 31st International Review of Progress in Applied Computational Electromagnetics; Willamsburg, W.Va. 2015.

Yan L, Waynert J, Sunderman C. Measurements and modeling of through-the-earth communications for coal mines. IEEE Trans Ind Appl. 2013; 49(5):1979–1983.

Yan, L., Zhou, C., Miguel, R., Whisner, B., Damiano, N. E-fields of electrode-based through-the-earth (TTE) communication. The IEEE IAS 2016 Meeting; Portland, Ore. 2016.

Appendix A

$$\frac{\partial^2 P}{\partial z^2}=\frac{e^{-\gamma R}}{R^2}\left(\frac{3z^2}{R^3}+\frac{3\gamma z^2}{R^2}-\frac{1}{R}+\frac{\gamma^2 z^2}{R}-\gamma\right) \quad \text{(A1)}$$

$$\frac{\partial^3 N}{\partial x\partial y\partial z}=A_{00}I_0K_0+A_{11}I_1K_1+A_{01}I_0K_1+A_{10}I_1K_0 \quad \text{(A2)}$$

$$\frac{\partial^3 N}{\partial y^2\partial z}=\frac{\gamma}{2}(B_{00}I_0K_0+B_{11}I_1K_1+B_{01}I_0K_1+B_{10}I_1K_0) \quad \text{(A3)}$$

$$\frac{\partial^2 P}{\partial x \partial z} = \frac{e^{-\gamma R}(x - \mathrm{x}')z}{R^3}\left(\frac{3}{R^2} + \frac{3\gamma}{R} + \gamma^2\right) \quad \text{(A4)}$$

where

$$A_{00} = \frac{-3(x-x')yz\gamma^2}{2R^4}$$
$$A_{11} = \frac{yz\gamma^2(x-x')(5R^2-3z^2)}{2R^4(R^2-z^2)}$$
$$A_{01} = -\frac{y\gamma(x-x')(3(z-R)+zR^2\gamma^2)}{2R^5}$$
$$A_{10} = \frac{y\gamma(x-x')(3(z+R)+zR^2\gamma^2)}{2R^5}$$
$$B_{00} = \frac{\gamma z}{R^2}\left(1 - \frac{3y^2}{R^2}\right)$$
$$B_{11} = \frac{\gamma z}{R^2}\left(-1 + \frac{3y^2}{R^2} + \frac{2y^2}{\rho^2}\right)$$
$$B_{01} = \frac{1}{R^2}\left(-1 + \frac{z(1-\gamma^2 y^2)}{R} + \frac{3y^2}{R^2} - \frac{3zy^2}{R^3}\right)$$
$$B_{10} = \frac{1}{R^2}\left(-1 - \frac{z(1-\gamma^2 y^2)}{R} + \frac{3y^2}{R^2} + \frac{3zy^2}{R^3}\right)$$

and I_1 is the modified Bessel functions of the first kind of order one, with the argument of $(R + z)\gamma/2$; K_1 is the modified Bessel functions of the second kind of order one, with the argument of $(R-z)\gamma/2$.

Key Points

- A three-dimensional model of the electric field distribution of electrode-based TTE communication was developed
- Optimal operating frequency found in both model predication and test data
- Signal reciprocity between surface and underground in electrode-based TTE communication was observed

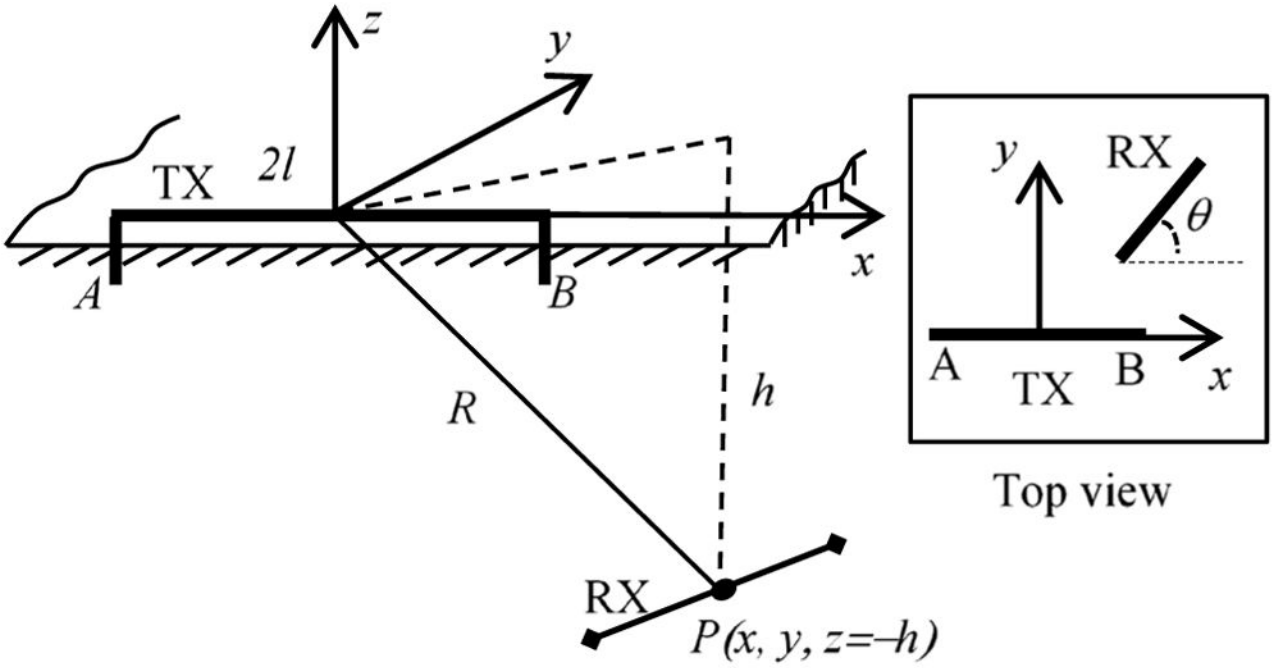

Figure 1.

A current carrying cable situates at ground. It has a length of 2 *l*. The observation point *P* (or the RX) is located at $z = -h$ homogenous subsurface. The TX and RX have an orientation angle θ.

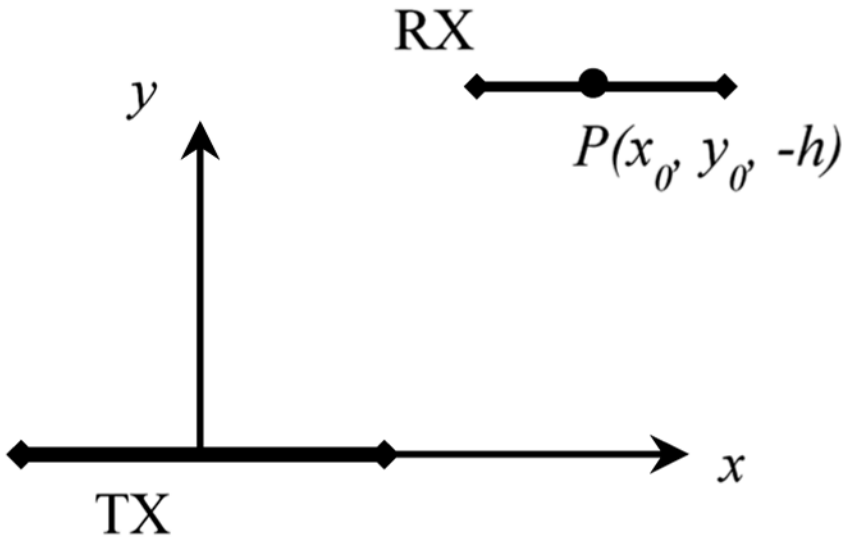

Figure 2.

Top view of TX/RX with parallel offset y_0 in y direction and coaxial offset x_0 in x direction. The RX center is located at $P(x_0, y_0, z = -h)$. The TX and RX are vertically separated with distance h.

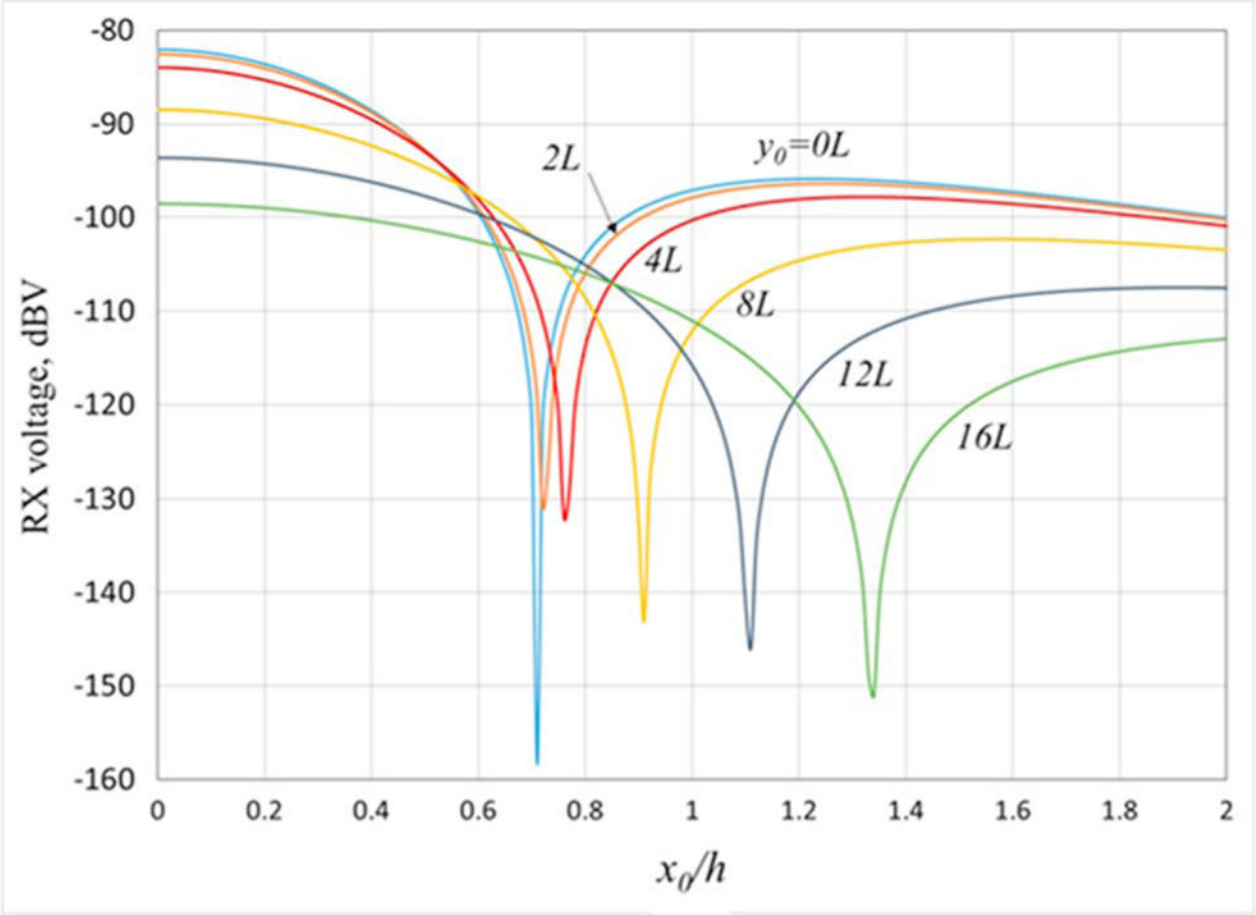

Figure 3.

Voltage at receiver changes with TX/RX coaxial distance (x_0/h) for various offsets y_0. h = 200 m, L = 20 m, σ = 0.1 S/m, and I = 1A.

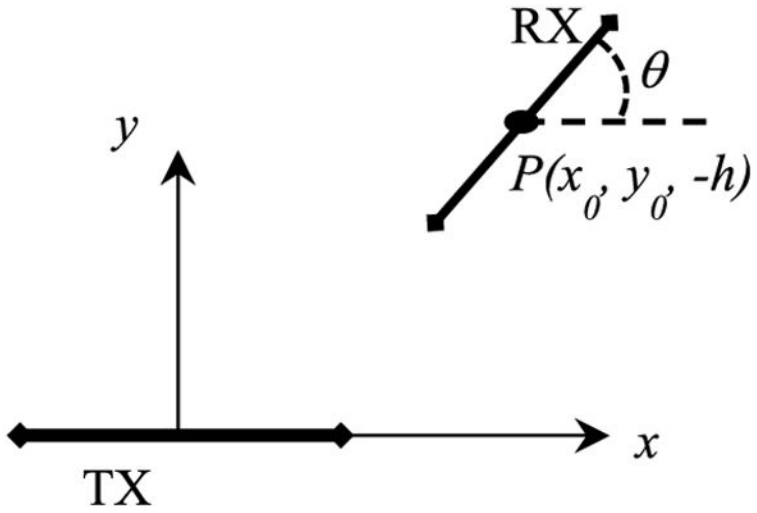

Figure 4.

Top view of TX/RX with intersection angle θ. The RX center is located at $P(x_0, y_0, z = -h)$. The TX and RX are vertically separated with distance h.

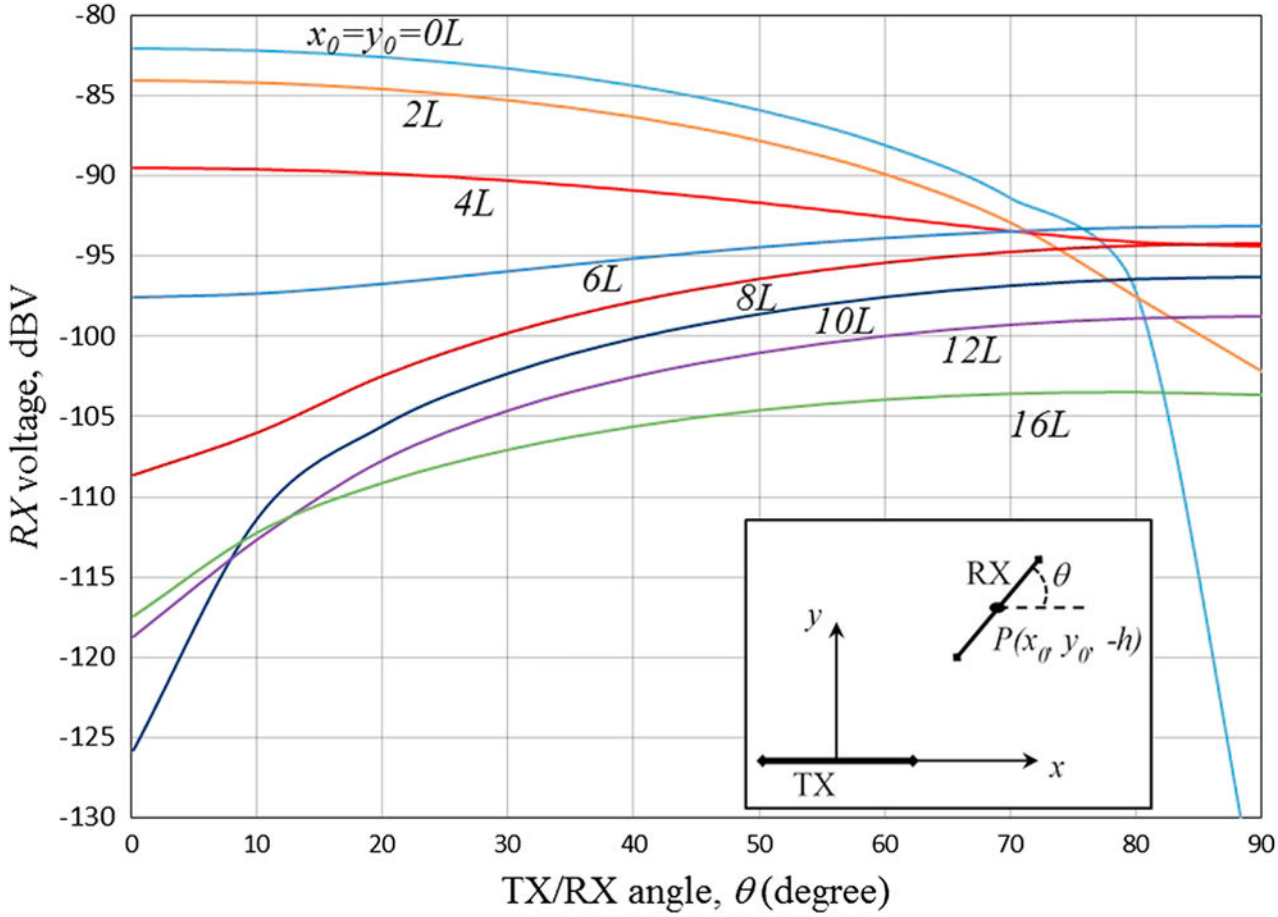

Figure 5.

Voltage at receiver changes with TX/RX intersection angle (θ) at various P locations. h = 200 m, L = 20 m, σ = 0.1 S/m, and I = 1A.

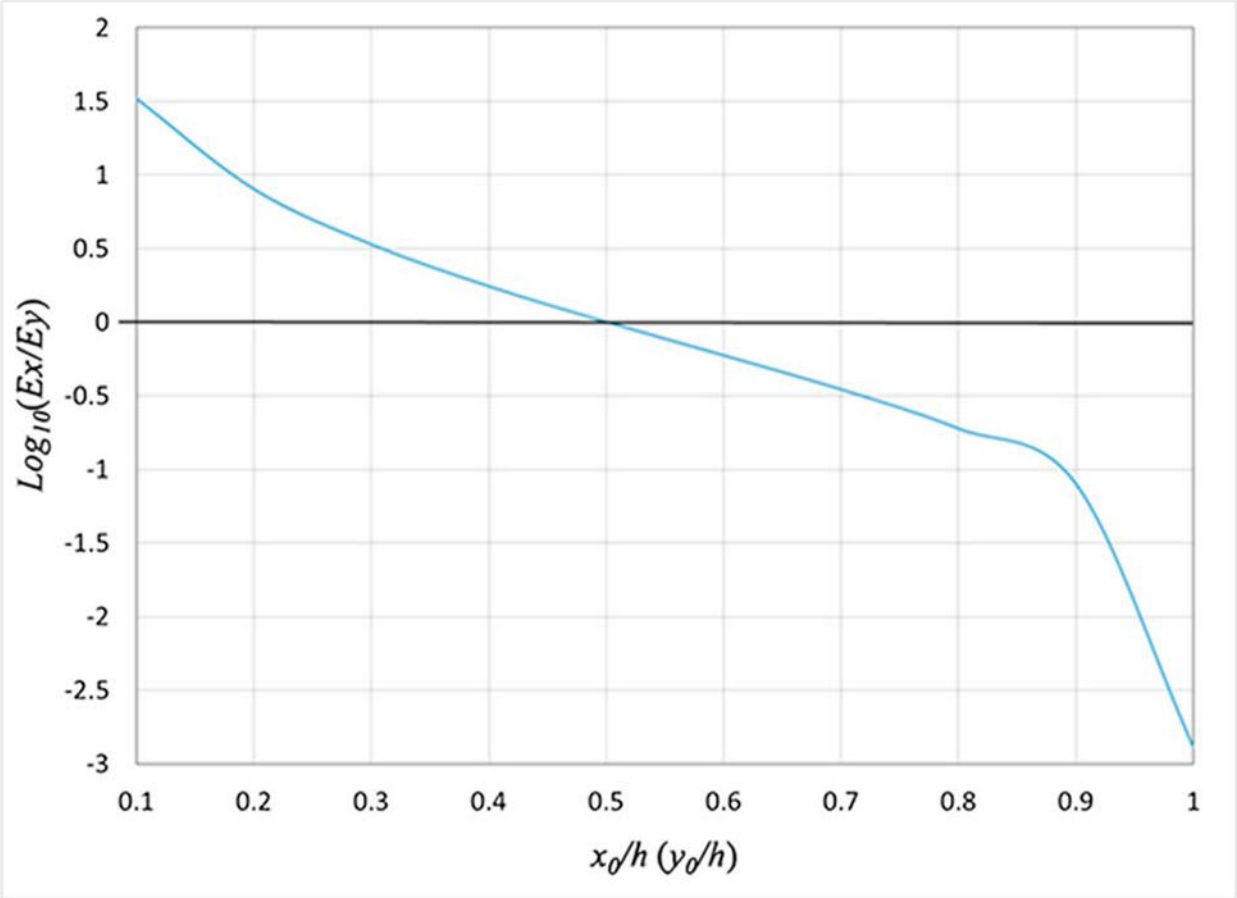

Figure 6.

Ratio of *x*-component *E* field to *y*-component *E* field changing with *P* locations. $x_0 = y_0$, $h =$ 200 m, $L = 20$ m, $\sigma = 0.1$ S/m, and $I = 1$A.

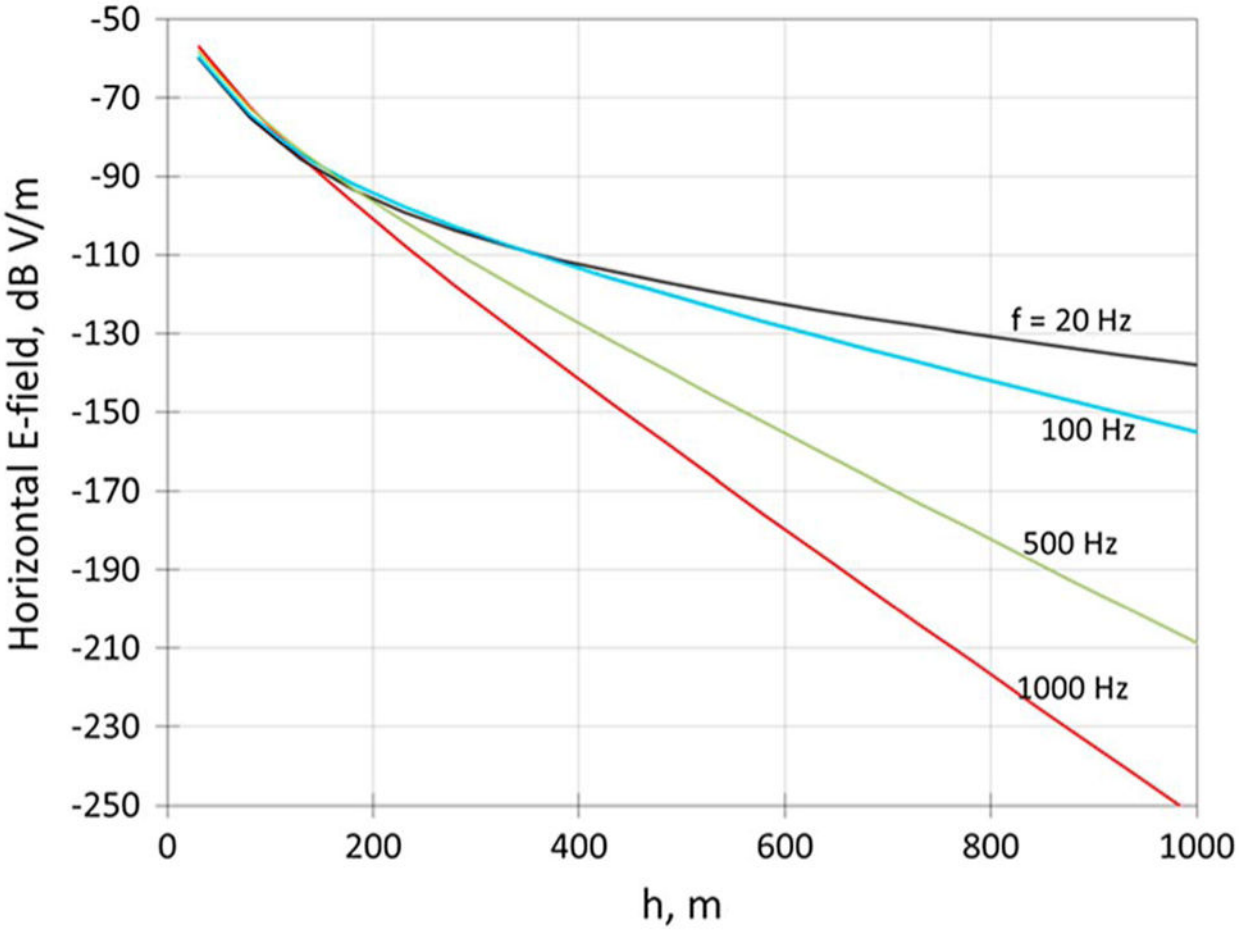

Figure 7.

Horizontal E field (normalized) varies with mine overburden depth, h, at different frequencies. The other parameters used are $x = 0$, $y = 0$, $\sigma = 0.05$ S/m, and $L = 76$ m.

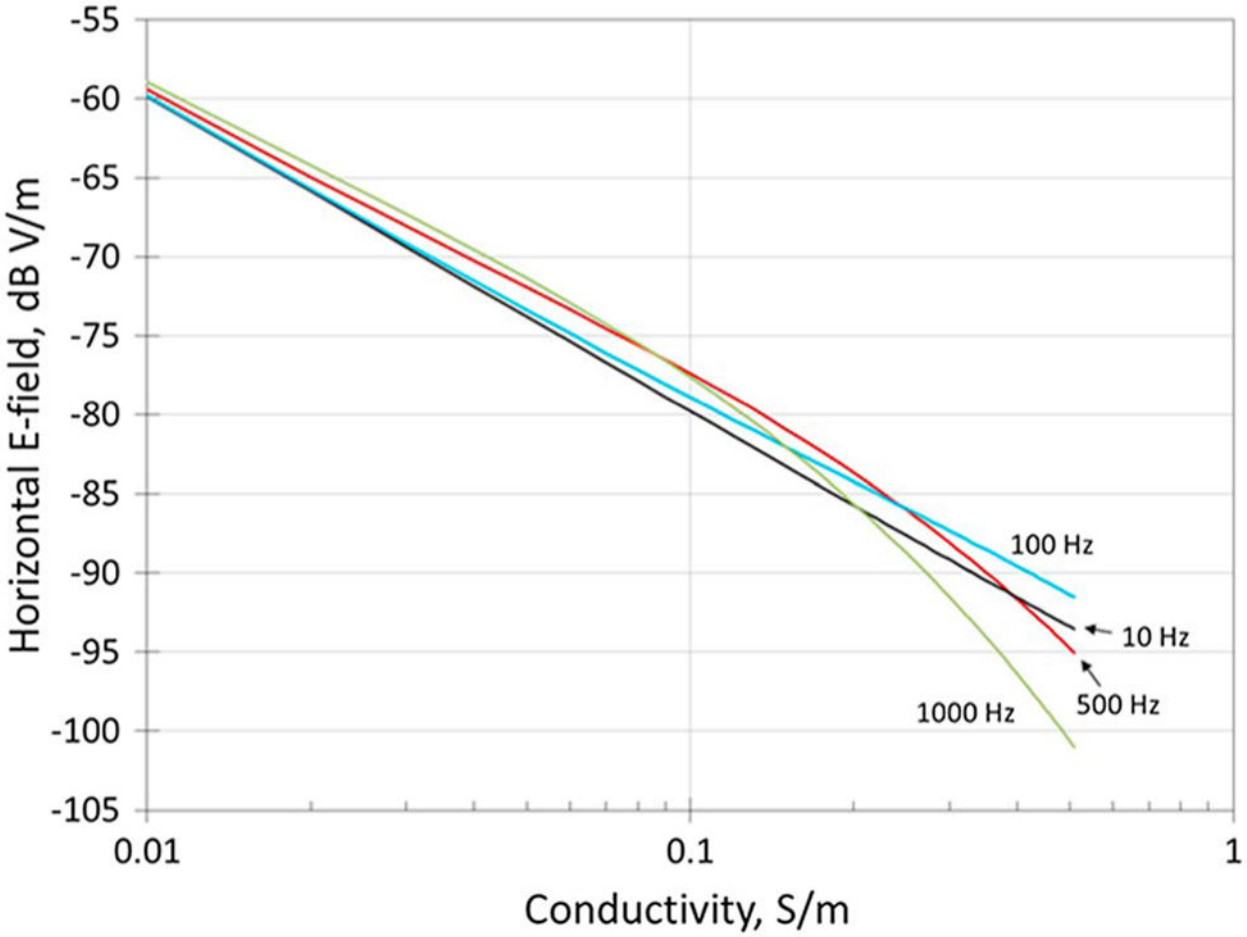

Figure 8.

Horizontal E field (normalized) varies with apparent earth conductivity at different frequencies. The other parameters used are $x = 0$, $y = 0$, $z = -h = -100$ m, and L = 76 m.

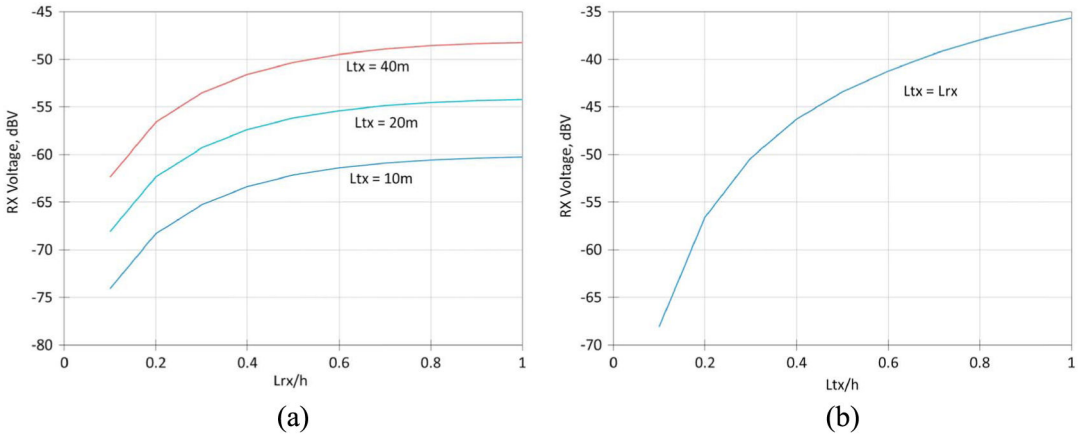

Figure 9.

RX voltage changes with (a) RX length (2Lrx) for different TX length (2Ltx) and (b) TX length (2Ltx = 2Lrx). $x = 0$, $y = 0$, $z = -h = -200$ m, $\sigma = 0.05$ S/m, and $f = 300$ Hz.

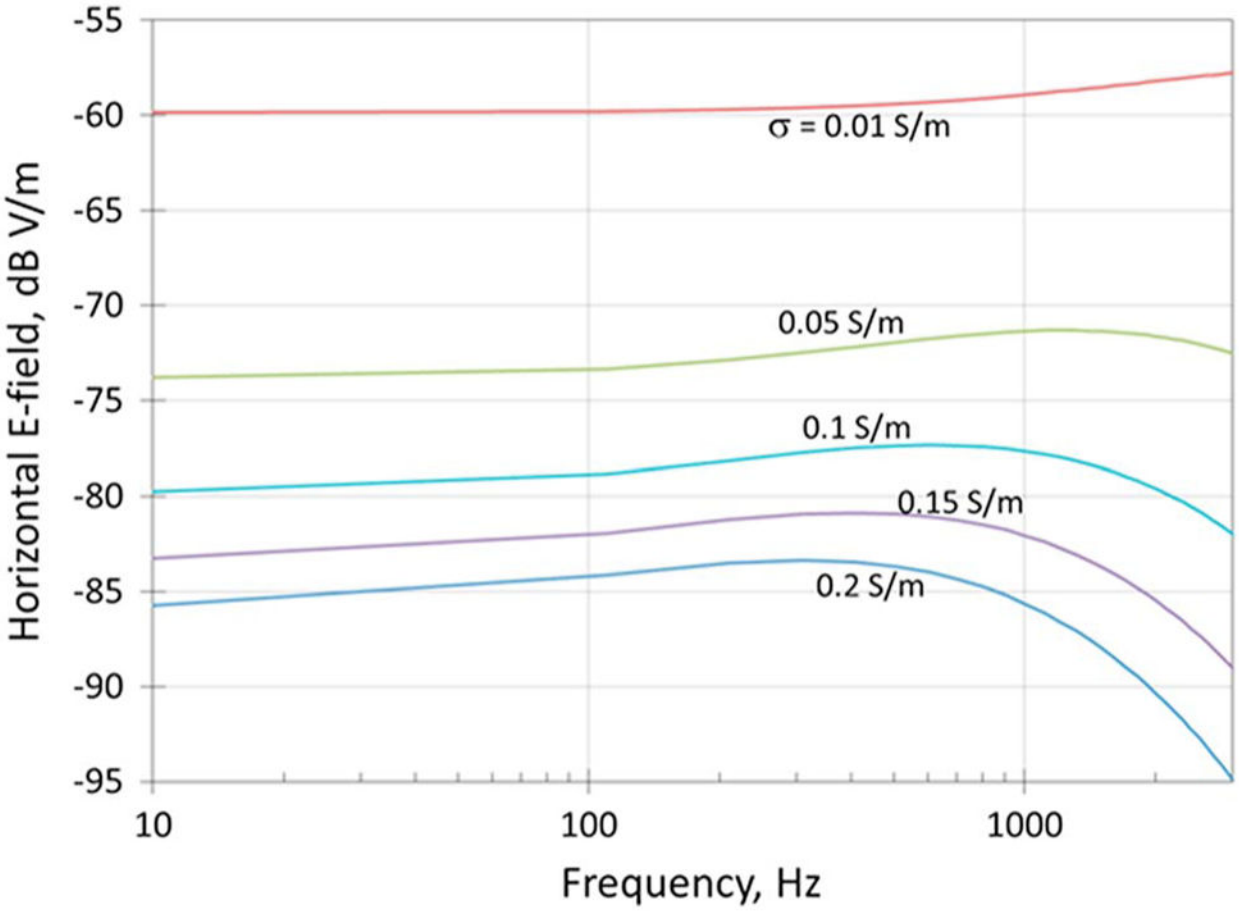

Figure 10.

Underground horizontal *E* field (normalized) varies with operating frequency at different apparent conductivities. $x = 0$, $y = 0$, and $z = -h = -100$ *m.*

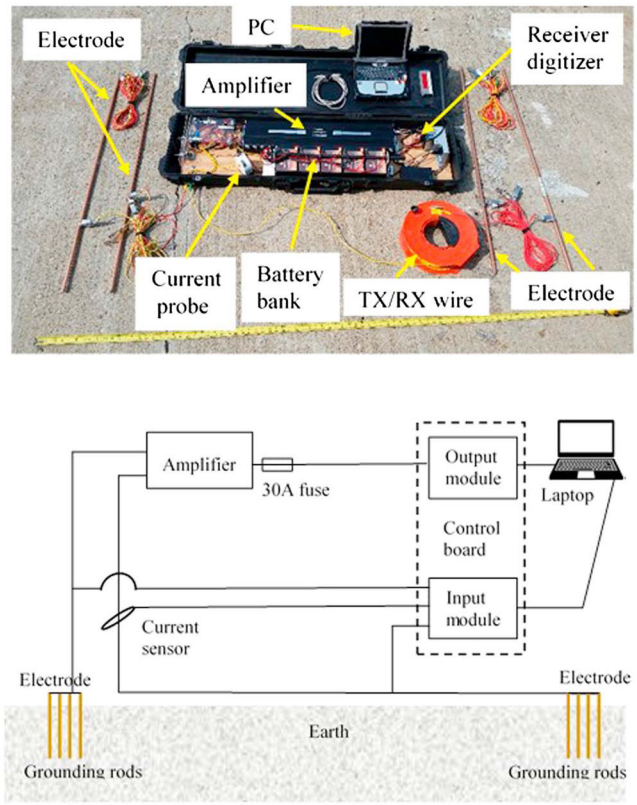

Figure 11.
Electrode-based TTE system (upper) and block diagram (lower).

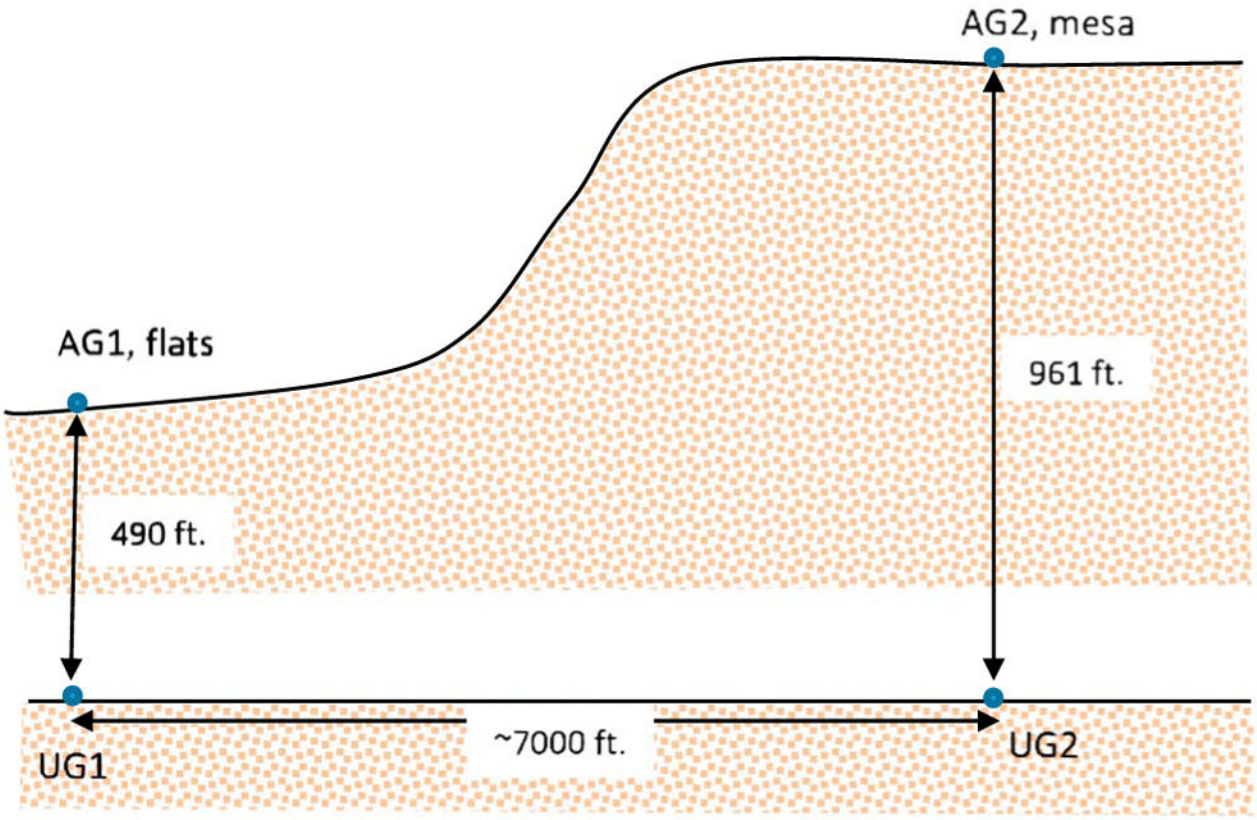

Figure 12.
Test locations—two underground and two surface.

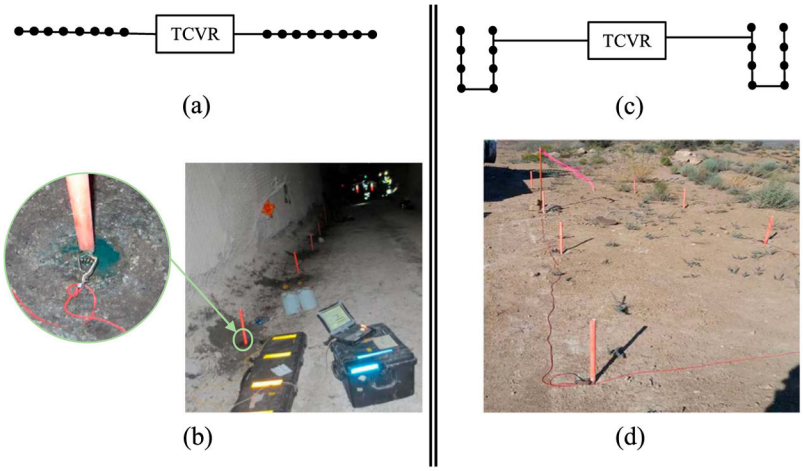

Figure 13.
(a and b) Underground and (c and d) surface electrode deployment with transceiver (TCVR).

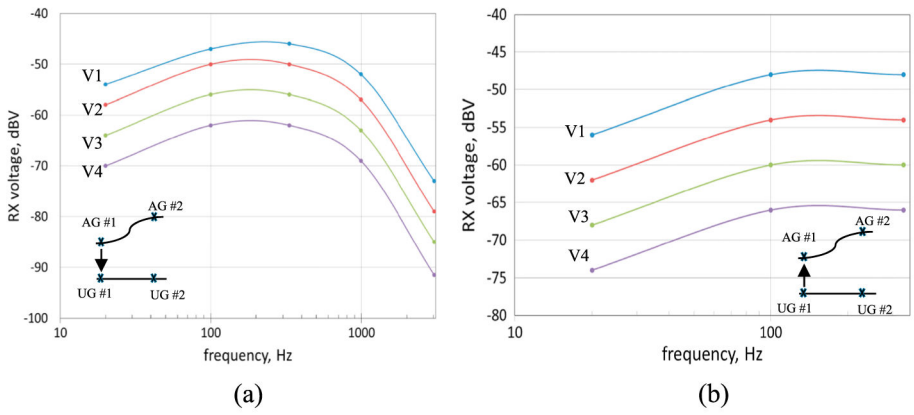

Figure 14.

Received voltage at RX corresponds to various frequencies at different transmitting current V1 through V4, for (a) downlink from AG1 to UG1 and (b) uplink from UG1 to AG1 at Location 1.

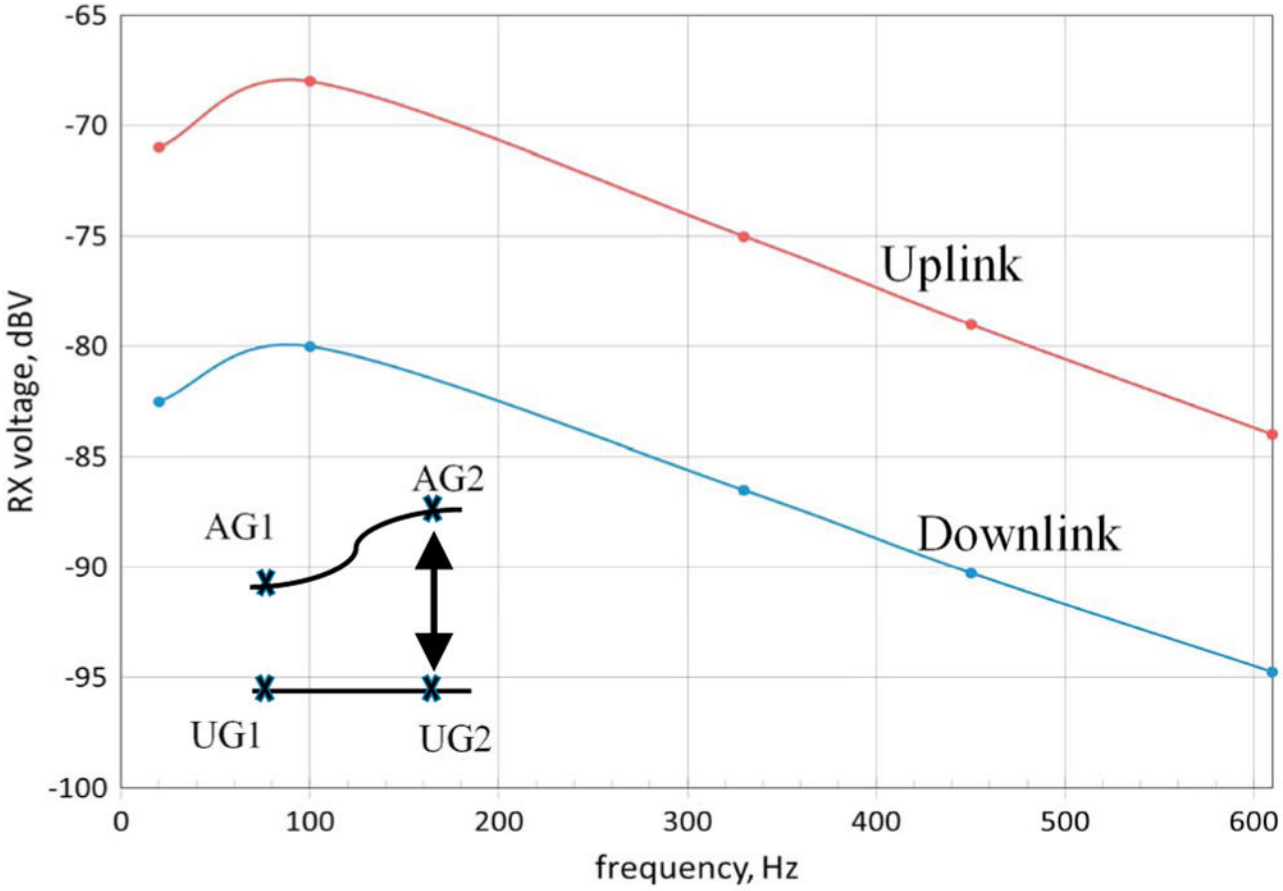

Figure 15.
Received voltage at RX corresponds to various frequencies for downlink and uplink transmission at Location 2.

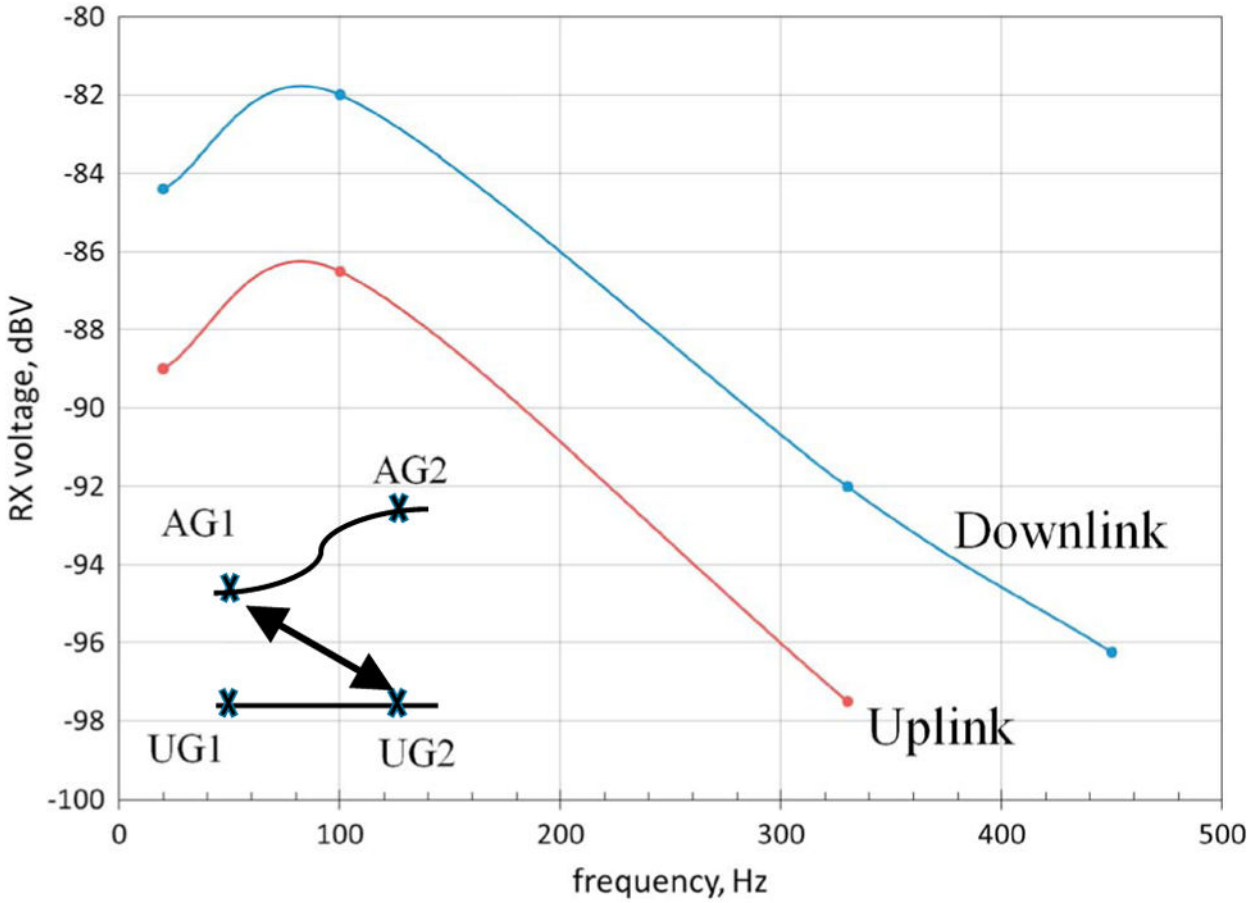

Figure 16.
Received voltage at RX corresponds to various frequencies for downlink and uplink between AG1 and UG2.

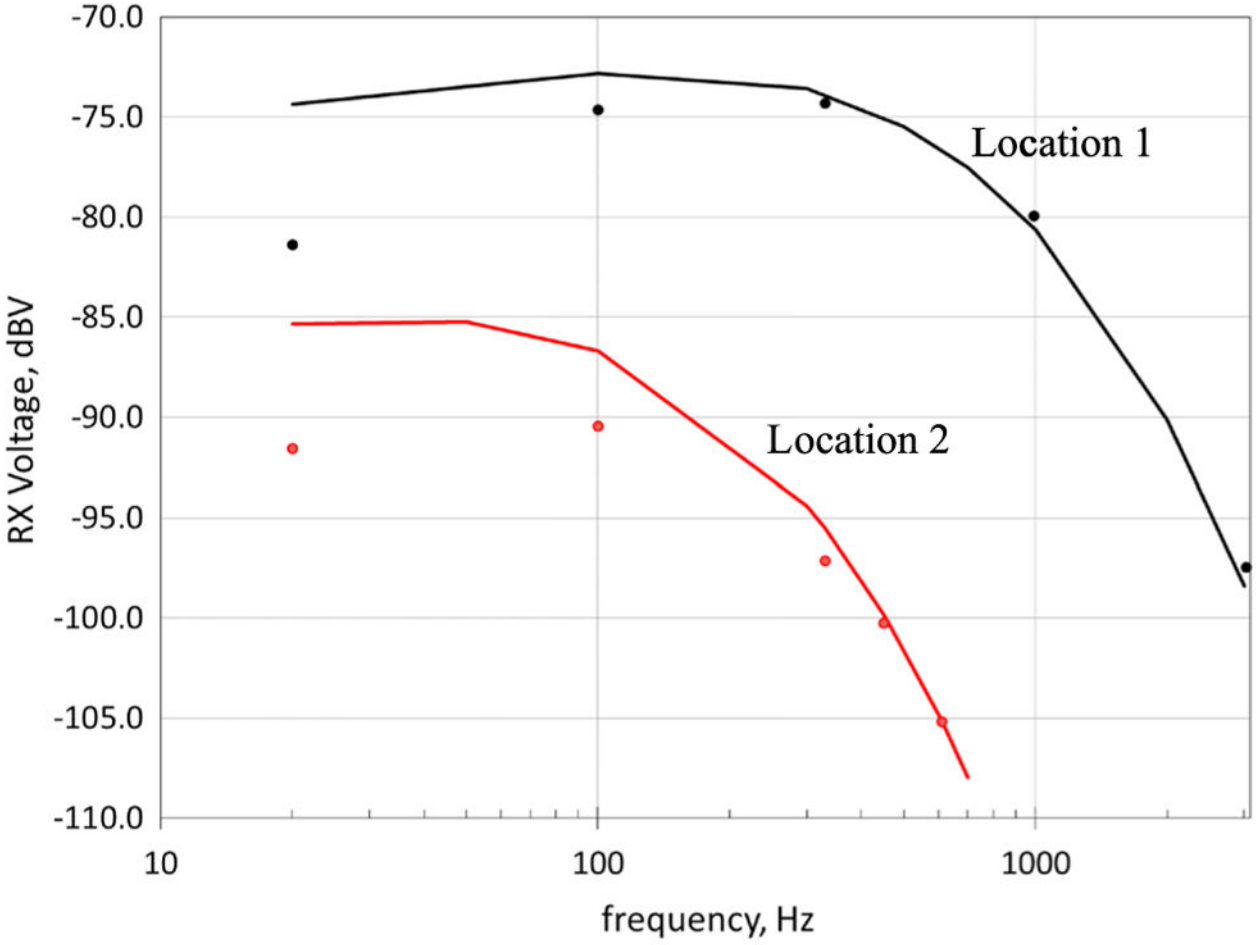

Figure 17.
Normalized RX voltage ($\boldsymbol{V_{RX}/I_{TX}}$) for model prediction (solid lines) and test data (dots) at different locations. σ = 0.2 S/m, antenna length 2 l = 76m.

Table 1

Earth Resistance Between Electrodes at Different Test Locations

Location	AG1	AG2	UG1	UG2
Earth resistance (Ω	1.8	35	2.0	7.0

Table 2

RX Voltage (Normalized by Transmitting Current *I*) for Uplink and Downlink Transmission at All Test Conditions Link Between Frequency (Hz) $V_{\mathbf{RX}}/I_{\mathrm{TX}}$, dBV Downlink $V_{\mathrm{RX}}/I_{\mathrm{TX}}$, dBV Uplink Difference (%)

Link Between	Frequency (Hz)	V_{RX}/I_{TX}, dBV Downlink	V_{RX}/I_{TX}, dBV Uplink	Difference (%)
AG1 and UG1	20	−81.4	−81.3	0.1
	100	−74.6	−74.5	0.2
	330	−74.3	−74.4	0.1
AG2 and UG2	20	−91.6	−91.9	0.3
	100	−90.5	−90.0	0.5
	330	−97.1	−96.9	0.2
	450	−100.2	−100.2	0.0
	610	−105.2	−105.6	0.4
AG1 and UG2	20	−111.4	−112.4	0.8
	100	−110.1	−110.9	0.7
	330	−120.9	−121.8	0.7